

Photonic crystal molecules: tailoring the coupling strength and sign

S. Haddadi, Philippe Hamel, G. Beaudoin, Isabelle Sagnes, Christophe Sauvan, Philippe Lalanne, Juan Ariel Levenson, Alejandro M. Yacomotti

▶ **To cite this version:**

S. Haddadi, Philippe Hamel, G. Beaudoin, Isabelle Sagnes, Christophe Sauvan, et al.. Photonic crystal molecules: tailoring the coupling strength and sign. Optics Express, 2014, 22 (10), pp.12359-12368. 10.1364/OE.22.012359 . hal-00993238

HAL Id: hal-00993238

https://hal-iogs.archives-ouvertes.fr/hal-00993238

Submitted on 21 May 2014

HAL is a multi-disciplinary open access archive for the deposit and dissemination of scientific research documents, whether they are published or not. The documents may come from teaching and research institutions in France or abroad, or from public or private research centers.

L'archive ouverte pluridisciplinaire **HAL**, est destinée au dépôt et à la diffusion de documents scientifiques de niveau recherche, publiés ou non, émanant des établissements d'enseignement et de recherche français ou étrangers, des laboratoires publics ou privés.

Photonic molecules: tailoring the coupling strength and sign

S. Haddadi,[1] P. Hamel,[1] G. Beaudoin,[1] I. Sagnes,[1] C. Sauvan,[2] P. Lalanne,[3] J. A. Levenson,[1] and A. M. Yacomotti[1,*]

[1]*Laboratoire de Photonique et de Nanostructures (CNRS UPR20), Route de Nozay, 91460 Marcoussis, France*

[2]*Laboratoire Charles Fabry, Institut d'Optique Graduate School, CNRS, Univ. Paris Sud, 2 avenue Augustin Fresnel, F-91127 Palaiseau, France*

[3]*Laboratoire Photonique Numérique et Nanosciences, Institut d'Optique d'Aquitaine, Université Bordeaux, CNRS, 33405 Talence, France*

[*]*Alejandro.Giacomotti@lpn.cnrs.fr*

Abstract: We demonstrate a large tuning of the coupling strength in Photonic Crystal molecules without changing the inter-cavity distance. The key element for the design is the "photonic barrier engineering", where the "potential barrier" is formed by the air-holes in between the two cavities. This consists in changing the hole radius of the central row in the barrier. As a result we show, both numerically and experimentally, that the wavelength splitting in two evanescently-coupled Photonic Crystal L3 cavities (three holes missing in the ΓK direction of the underlying triangular lattice) can be continuously controlled up to $5\times$ the initial value upon $\sim 30\%$ of hole-size modification in the barrier. Moreover, the sign of the splitting can be reversed in such a way that the fundamental mode can be either the symmetric or the anti-symmetric one without altering neither the cavity geometry nor the inter-cavity distance. Coupling sign inversion is explained in the framework of a Fabry-Perot model with underlying propagating Bloch modes in coupled W1 waveguides.

© 2014 Optical Society of America

OCIS codes: (350.4238) Nanophotonics and photonic crystals; (140.3945) Microcavities.

References and links

1. S. Boriskina, "Photonic molecules and spectral engineering," in *Photonic Microresonator Research and Applications*, Vol. 156, I. Chremmos, O. Schwelb, and N. Uzunoglu, eds. (Springer, 2010) pp. 393–421.
2. L. Shang, L. Liu, and L. Xu, "Single-frequency coupled asymmetric microcavity laser," Opt. Lett. **33**, 1150–1152 (2008).
3. M. Notomi, E. Kuramochi, and T. Tanabe, "Large-scale arrays of ultrahigh-Q coupled nanocavities," Nat. Photon. **2**, 741 (2008).
4. Y. Sato, Y. Tanaka, J. Upham, Y. Takahashi, T. Asano, and S. Noda, "Strong coupling between distant photonic nanocavities and its dynamic control," Nat. Photon. **6**, 56–61 (2012).
5. X. Yang, M. Yu, D. L. Kwong, and C. W. Wong, "All-optical analog to electromagnetically induced transparency in multiple coupled photonic crystal cavities," Phys. Rev. Lett. **102**, 173902 (2009).
6. D. Gerace, H. E. Türeci, A. Imamoglu, V. Giovannetti, and R. Fazio, "The quantum-optical Josephson interferometer," Nat. Phys. **5**, 281–284 (2009).
7. A. Majumdar, A. Rundquist, M. Bajcsy, and J. Vuckovic, "Cavity quantum electrodynamics with a single quantum dot coupled to a photonic molecule," Phys. Rev. B **86**, 045315 (2012).
8. A. M. Yacomotti, S. Haddadi, and S. Barbay, "Self-pulsing nanocavity laser," Phys. Rev. A **87**, 041804(R) (2013).

#210083 - $15.00 USD Received 14 Apr 2014; accepted 25 Apr 2014; published 13 May 2014
(C) 2014 OSA

9. M. Abbarchi, A. Amo, V. G. Sala, D. D. Solnyshkov, H. Flayac, L. Ferrier, I. Sagnes, E. Galopin, A. Lemaître, G. Malpuech, and J. Bloch, "Macroscopic quantum self-trapping and Josephson oscillations of exciton polaritons," Nat. Phys. **9**, 275–279 (2013).
10. B. A. Malomed, ed., *Spontaneous Symmetry Breaking, Self-Trapping, and Josephson Oscillations* (Springer, 2013).
11. M. Brunstein, T. J. Karle, I. Sagnes, F. Raineri, J. Bloch, Y. Halioua, G. Beaudoin, L. Le Gratiet, J. A. Levenson, and A. M. Yacomotti, "Radiation patterns from coupled photonic crystal nanocavities," Appl. Phys. Lett. **99**, 111101 (2011).
12. N. Caselli, F. Intonti, F. Riboli, A. Vinattieri, D. Gerace, L. Balet, L. H. Li, M. Francardi, A. Gerardino, A. Fiore, and M. Gurioli, "Antibonding ground state in photonic crystal molecules," Phys. Rev. B **86**, 035133 (2012).
13. Y. Akahane, T. Asano, B. S. Song, and S. Noda, "High-Q photonic nanocavity in a two-dimensional photonic crystal," Nature **425**, 944–947 (2003).
14. S. Haddadi, L. Le Gratiet, I. Sagnes, F. Raineri, A. Bazin, K. Bencheikh, J. A. Levenson, and A. M. Yacomotti, "High quality beaming and efficient free-space coupling in L3 photonic crystal active nanocavities," Opt. Express **20**, 18876–18886 (2012).
15. S. Haddadi, A. M. Yacomotti, I. Sagnes, F. Raineri, G. Beaudoin, L. Le Gratiet, and J. A. Levenson, "Photonic crystal coupled cavities with increased beaming and free space coupling efficiency," Appl. Phys. Lett. **102**, 011107 (2013).
16. K. A. Atlasov, K. F. Karlsson, A. Rudra, B. Dwir, and E. Kapon, "Wavelength and loss splitting in directly coupled photonic-crystal defect microcavities," Opt. Express **16**, 16255–16264 (2008).
17. S. Ishii, K. Nozaki, and T. Baba, "Photonic molecules in photonic crystals," Jpn. J. Appl. Phys. **45**, 6108 (2006).
18. A. R. A. Chalcraft, S. Lam, B. D. Jones, D. Szymanski, R. Oulton, A. C. T. Thijssen, M. S. Skolnick, D. M. Whittaker, T. F. Krauss, and A. M. Fox, "Mode structure of coupled L3 photonic crystal cavities," Opt. Express **19**, 5670–5675 (2011).
19. N. Caselli, F. Intonti, F. Riboli, and M. Gurioli, "Engineering the mode parity of the ground state in photonic crystal molecules," Opt. Express **22**, 4953–4959 (2014).
20. G. Lecamp, J. P. Hugonin, and P. Lalanne, "Theoretical and computational concepts for periodic optical waveguides," Opt. Express **15**, 11042–11060 (2007).
21. The terms symmetric and antisymmetric correspond to the symmetry of the longitudinal electric field component (parallel to the ΓK direction).
22. C. Sauvan, P. Lalanne, and J. P. Hugonin, "Slow-wave effect and mode-profile matching in photonic crystal microcavities," Phys. Rev. B **71**, 165118 (2005).
23. B. S. Song, S. Noda, T. Asano, and Y. Akahane, "Ultra-high-Q photonic double-heterostructure nanocavity," Nat. Mater. **4**, 207–210 (2005).

1. Introduction

Coupled micro and nanocavities, also called photonic molecules [1], are being investigated with increasing interest due to their relevance in applications such as laser optimization [2], delay lines [3], optical strong coupling [4], optical equivalent of EIT [5], as well as a testbed for the exploration of advanced nonlinear and quantum regimes [6–8]. In this context, evanescently coupled optical cavities can be regarded as multiple potential well systems which, in the presence of nonlinearities, may allow the demonstration of fundamental phenomena such as Josephson oscillations, optical self-trapping or even spontaneous symmetry breaking [9, 10]. For both the demonstration of novel physical regimes and applications, a key issue is the control of the coupling strength. A control parameter able to drive the coupled cavity system from weak to strong coupling regimes without completely modifying the nature of the photonic molecule is largely desirable. Moreover, optical systems allow, in principle, to change not only the strength of the evanescent interaction but also its sign. Although this is not a typical feature in standard micro cavities such as micro pillars, micro disks or microtoroids, reverse coupling situations have already been observed for instance in coupled photonics crystal (PhC) nanocavities [11, 12].

Among the diversity of possible geometries of micro and nanocavities, PhCs give rise to a substantial versatility in the choice of design parameters. For instance, it is well-known that small changes in neighbor holes of a PhC cavity, such a L3 cavity (three holes missing in the ΓK direction of a triangular lattice), may boost the quality (Q) factor for more than one order of

#210083 - $15.00 USD Received 14 Apr 2014; accepted 25 Apr 2014; published 13 May 2014
(C) 2014 OSA

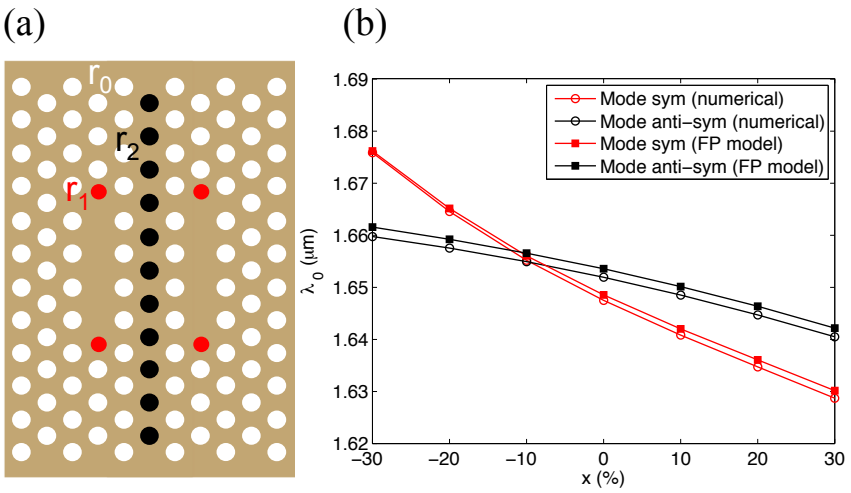


Fig. 1. Barrier engineering: 2D model. (a) Schematics of two coupled L3 cavities with modified barrier. Refractive index is $n = 2.77$, lattice period $a = 0.430\,\text{nm}$, hole radius of the PhC triangular lattice $r_0 = 0.266a$ (white holes), size of shifted holes $r_1 = r_0 - 0.06a$ (red holes), and the radius of modified holes within the barrier (black holes) is $r_2 = r_0(1+x)$. (b) Numerical results of resonant wavelengths for symmetric (red) and antisymmetric (black) modes, as a function of the barrier hole size x. Filled squares: results from the Fabry-Perot model; open circles: direct numerical calculation of resonant wavelengths.

magnitude [13]. In addition, PhC cavities can be tailored to improve the beaming properties [14, 15]. In the context of coupled cavities, PhCs give a handle to the easy and robust engineering of both the strength and the nature –conservative or dissipative– of the inter-cavity coupling [16]. The observable quantity associated to such coupling strength is the mode splitting, which has been largely studied in a variety of PhC geometries and coupling configurations [17, 18].

Several attempts to control frequency splitting in PhC coupled cavities have been carried out in the recent years. As a general rule, the distance between point-defect-cavities, which can be varied in a discrete manner only, controls the mode splitting. Therefore, bonding and anti-bonding modes will approach each other for distant cavities, or separate away for close enough defects [18]. In addition, specific coupling configurations may spectrally locate the anti-bonding modes either at the blue or at the red side of the bonding modes. In other words, the coupling sign can be reversed in PhC molecules [11, 12]. The ability of PhCs to give rise to anti-bonding ground states has been discussed in [12], in the framework of two-coupled D2 (four missing holes) PhC cavities. Recently, a theoretical study has been carried out on the same D2 molecules in order to show that the parity of the ground state can be changed [19].

In this paper we carry out, both numerically and experimentally, specific barrier engineering of two coupled L3 cavities leading to a continuous control of mode splitting together with the inversion of the coupling sign, all this at a fixed distance between the cavities. We also numerically show that the use of L3 optical defects makes this technique compatible with high Q-factor ($Q \sim 5 \times 10^4$) nano-cavities.

2. Barrier engineering: Fabry Perot model for a 2D system

In order to introduce the concept of barrier engineering, we first consider PhC molecules in a two-dimensional (2D) PhC. The system consists of two coupled L3 cavities as optical defects in the ΓK direction, separated by three rows of holes in the ΓM direction [Fig. 1(a)]. The effective

#210083 - $15.00 USD Received 14 Apr 2014; accepted 25 Apr 2014; published 13 May 2014
(C) 2014 OSA

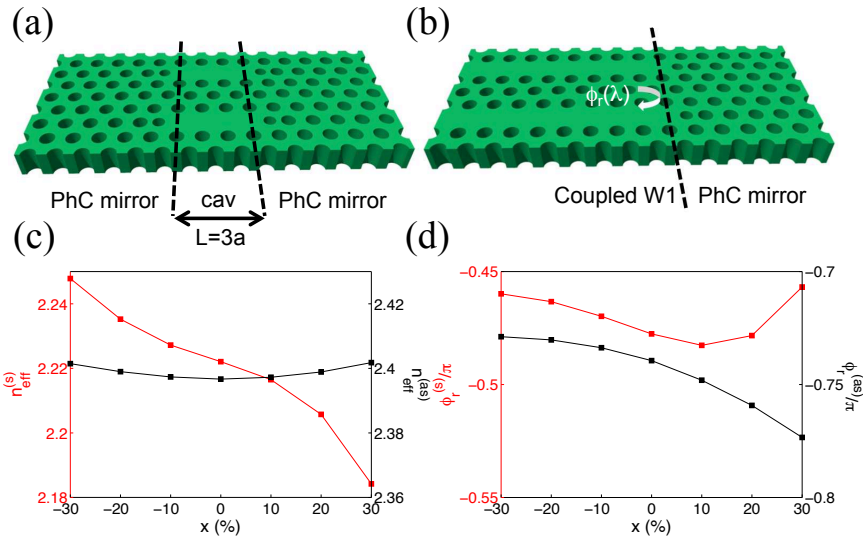


Fig. 2. Building-up the Fabry-Perot model. (a) An optical defect is composed by a "free propagation" cavity region of length $L = 3a$ surrounded by two PhC mirrors; the boundary between the cavity region and the mirror is given by the dashed lines. (b) Phase of the modal reflection $[\phi_r(\lambda)]$ of the Bloch modes of two coupled W1 waveguides on a PhC mirror. (c) Effective index of symmetric (red) and anti-symmetric (black) Bloch modes. The values of the effective index are taken at the resonance wavelengths of the cavities. (d) Idem as in (c) for the reflectivity phases at resonance.

index ($n = 2.77$) chosen for the 2D PhC corresponds to the effective index of a planar InP membrane of thickness $e = 265\,\text{nm}$ at $\lambda = 1.55\,\mu\text{m}$. The period and hole radius of the underlying triangular PhC lattice are $a = 430\,\text{nm}$ and $r_0 = 0.266a$, respectively. The two end-holes of each cavity are separated away by $s = 0.16a$ and their radius is reduced to $r_1 = r_0 - 0.06a$ in order to increase the Q-factor of the 3D-system (Fig. 1(a), red holes); their influence is negligible within this 2D representation. Our scheme for barrier engineering consists in modifying the hole size of the central row in the barrier (Fig. 1(a), black holes), whose radius becomes $r_2 = r_0(1+x)$.

The aperiodic Fourier Modal Method (a-FMM) [20] has been used in order to compute eigenmode frequencies of the coupled cavities. Symmetric (red) and antisymmetric (black) resonant wavelengths $\lambda_0^{(s)}$ and $\lambda_0^{(as)}$ are plotted in Fig. 1(b) as a function of radius change x [21]. We observe: i) for $x = 0$, the anti-symmetric mode is the one with longer wavelength (i.e. antisymmetric ground state), which has been already observed in previous works, both experimentally and numerically for L3 cavities [11, 15]; ii) the mode splitting is a function of x, and a global blueshift of modes as x is increased is observed; iii) there is a degeneracy point at $x = x_c \sim -10\%$ which separates two distinct regions: for $x > x_c$ the splitting progressively increases, with the same spectral order $\lambda_0^{(as)} > \lambda_0^{(s)}$ as in (i), whether for $x < x_c$ the spectral order is reversed and now the symmetric mode is the one with longer wavelength (i.e. symmetric ground state, $\lambda_0^{(s)} > \lambda_0^{(as)}$). We note that the latter is the typical situation found in classical and quantum mechanics and implies a given sign for the coupling parameter (say negative as in a Coupled Mode Theory framework), while in situation (i) the coupling sign is reversed and becomes positive. Hence, we have numerically shown that coupling strength and sign can be changed by simply varying the hole-radius of the central row of the barrier.

In order to explain this striking behavior, let us analyze the coupled-cavities system with a Fabry-Perot model based on the bouncing of a single Bloch mode in between two PhC mirrors,

#210083 - $15.00 USD Received 14 Apr 2014; accepted 25 Apr 2014; published 13 May 2014
(C) 2014 OSA

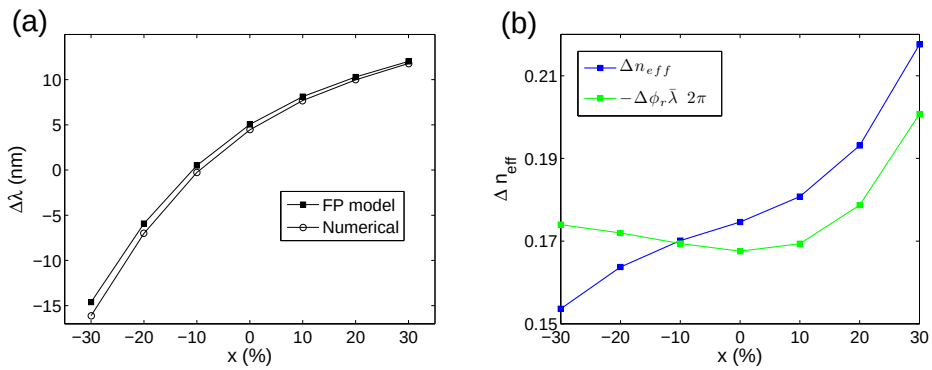


Fig. 3. (a) Wavelength splitting as a function of the hole size in the barrier. Filled squares: F-P model from Eq. (2); open circles: exact calculations. (b) Index (blue) and phase (green) contributions for the wavelength splitting. Degeneracy is achieved at the intersection of these two curves [see Eq. (3)].

see Figs. 2(a) and 2(b). For the symmetric (antisymmetric) cavity mode, we use the symmetric (antisymmetric) Bloch mode supported by the two coupled W1 waveguides. The model is a two-cavity extension of what has been proposed in the past to quantitatively explain Q-factor increase in single L3 cavities [22]. The a-FMM method used here allows us to compute propagation constants in periodic waveguides and their modal reflectances at waveguide terminations [20]. Specifically, we compute $k^{(s),(as)}(\lambda) = (2\pi/\lambda)n_{eff}^{(s),(as)}(\lambda)$ of the symmetric (s) and anti-symmetric (as) Bloch modes of the coupled W1 waveguides. A F-P cavity is formed by an optical defect, i.e. a waveguide region of length $L = 3a$, closed by two PhC mirrors with shifted end-holes [Fig. 2(a)]. Reflection of both Bloch modes onto the PhC is also computed with the a-FMM, which provides two complex reflectivity coefficients with phase $\phi_r^{(s),(as)}(\lambda)$ [Fig. 2(b)]. Phase matching conditions can then be written down for symmetric and anti-symmetric modes:

$$(2\pi/\lambda_0^{(s),(as)})n_{eff}^{(s),(as)}(\lambda_0^{(s),(as)})L + \phi_r^{(s),(as)}(\lambda_0^{(s),(as)}) = p\pi \tag{1}$$

where p is an integer (mode order, $p = 3$ for the resonance wavelength of interest). Resonant wavelengths as predicted by the F-P model are superimposed to the numerical results in Fig. 1(b). Equation (1) evidences that a blue-shift of the cavity mode may be due to a decrease of either the effective index (n_{eff}) or the reflectivity phase (ϕ_r).

Effective indices and phases at resonance are shown in Figs. 2(c) and 2(d). Increasing hole size (parameter x) blue-shifts the cavity modes (point (ii) above): for the symmetric mode, this is due to a decrease of $n_{eff}^{(s)}$, while the blue shift of the anti-symmetric one comes from a decrease of $\phi_r^{(as)}$. Let us now define averaged quantities and differences as $\bar{f} \equiv [f^{(as)} + f^{(s)}]/2$ and $\Delta f \equiv f^{(as)} - f^{(s)}$, where f can be n_{eff}, ϕ_r or λ. Equations (1) can be recast in the following way:

$$\Delta\lambda = \left(p - \frac{\bar{\phi_r}}{\pi}\right)^{-1}\left(2L\Delta n_{eff} + \frac{\Delta\phi_r}{\pi}\bar{\lambda}\right). \tag{2}$$

Equation (2) relates wavelength splitting to effective index and phase differences. From Fig. 2(c) we remark that, unlike standard resonators such as micro rings and micropillars –built up from segments of uniform coupled waveguides–, the effective index of coupled W1 waveguides at cavity resonance is always larger for the antisymmetric mode compared to the symmetric one.

#210083 - $15.00 USD Received 14 Apr 2014; accepted 25 Apr 2014; published 13 May 2014
(C) 2014 OSA

A comparison of Eq. (2) with numerical results is shown in Fig. 3(a). For $x = 0$, i.e. no barrier modification, the effective index difference (first term in the r.h.s. of Eq. (2), positive) is slightly greater than the phase term (second term in the r.h.s. of Eq. (2), negative) in modulus, see Fig. 3(b). As a result $\Delta\lambda > 0$, and therefore $\lambda_0^{(as)} > \lambda_0^{(s)}$. We have thus shown that point (i) above (i.e. antisymmetric ground state for no barrier modification) is a direct consequence of the effective effective index of the antisymmetric mode being larger compared to the symmetric one.

Finally, degeneracy is achieved by setting $\Delta\lambda = 0$ in Eq. (2), which leads to

$$\Delta n_{eff} = -\frac{\Delta\phi_r \lambda_0}{2\pi L}, \tag{3}$$

where $\lambda_0 \equiv \bar{\lambda} = \lambda_0^{(s)} = \lambda_0^{(as)}$. Figure 3(b) shows that Eq. (3) is verified for $x \sim -10\%$ for which Δn_{eff} slightly decreases with respect to $x = 0$ in such a way that refractive index difference exactly compensates the phase difference. The main mechanism that allows degeneracy is that barrier engineering basically affects the effective index of one of the two modes (the symmetric one) while the other one remains essentially unchanged. Indeed, the middle row of holes being modified has a much stronger impact on the symmetric mode effective index for which the electric-field component does not vanish at the symmetry plane.

3. Barrier engineering: 3D numerical simulations

3D-Finite Difference Time Domain (FDTD) simulations have been performed in order to obtain a better approximation of the real system, as well as to account for optical losses, hence Q-factors in membrane-based cavities. Bulk material index is $n = 3.17$ and membrane thickness $e = 265\,\text{nm}$. Lattice period is $a = 390\,\text{nm}$ and $r_0 = 0.232a$. Other parameters (s and r_1) are the same as in Sec. 2, and we recall that $r_2 = r_0(1+x)$. Mirror symmetries have been exploited in order to reduce computation time. Mode frequencies and decay times (losses) are extracted from time-series data through a harmonic inversion algorithm. Wavelength splitting $\Delta\lambda = \lambda_0^{(as)} - \lambda_0^{(s)}$ as a function of x is shown in Figs. 4(a) and 4(b). As compared to the 2D simulations, the main features are preserved; mode crossing is now observed at $x_c \sim -0.08$. An initial splitting of $\Delta\lambda \sim 3\,\text{nm}$ is increased up to $\Delta\lambda \sim 9\,\text{nm}$ for $x = 0.3$, while it is reversed for $x < x_c$ and decreases down to $\Delta\lambda \sim -12\,\text{nm}$ for $x = -0.3$. The step size in x has been decreased close to the $\Delta\lambda = 0$ point: wavelength splitting as small as $\Delta\lambda = (30 \pm 15)\,\text{pm}$ have been obtained, limited by the resolution of the inversion algorithm, which identifies the crossing point [Fig. 4(b)]. Figure 5(a) shows that this crossing point is shifted towards smaller x-values as r_0 is increased; additional simulations (not shown) indicate that the results do not significantly depend on the period. Initial Q-factors ($x = 0$) are $Q_0^{(as)} \sim 65000$ and $Q_0^{(s)} \sim 55000$. We observe little variation –of the order of 10%– upon barrier modification. Q-factor as a function of hole change in the barrier is shown in the inset of Fig. 5(a).

Near field patterns (not shown) are close to those obtained for two coupled L3 cavities without barrier engineering. The only modification in the near field takes place for decreased hole radius ($x < 0$) for which the field intensity locally increases at the symmetry plane; this can be attributed to a refractive index effect as a result of the hole shrinking. Figures 6(a)–6(c) show far field patterns for different hole sizes in the barrier. Unlike near-field, far-field emission of the symmetric mode is (slightly) modified for increasing hole radius ($x > 0$) resulting in a broader emission pattern [Fig. 6(c)]. Changes in anti-symmetric mode patterns, in turn, are negligible. In the following experimental part, far-field patterns will be used as signatures of mode symmetry.

#210083 - $15.00 USD Received 14 Apr 2014; accepted 25 Apr 2014; published 13 May 2014
(C) 2014 OSA

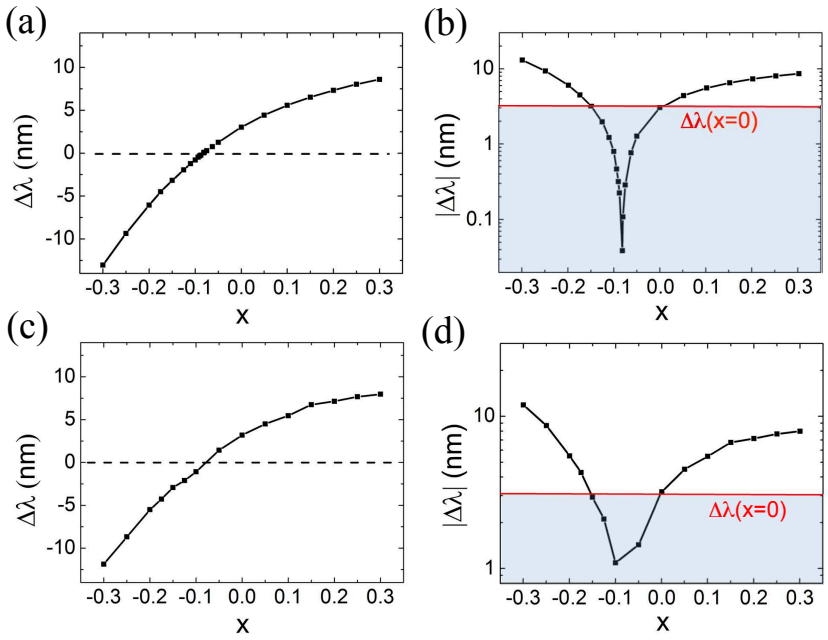


Fig. 4. (a) 3D-FDTD simulation results of wavelength splitting $\Delta\lambda = \lambda_0^{as} - \lambda_0^{s}$ as a function of the hole size in the barrier. (b) Modulus of (a) in log scale; red line is the initial splitting $[\Delta\lambda\,(x=0)]$. (c) and (d) Experimental results. Target parameters for the fabrication are the same as the theoretical ones, $a = 390\,\text{nm}$, $r_0 = 0.232a$, s=$0.16a$ and $r_1 = r_0 - 0.06a$.

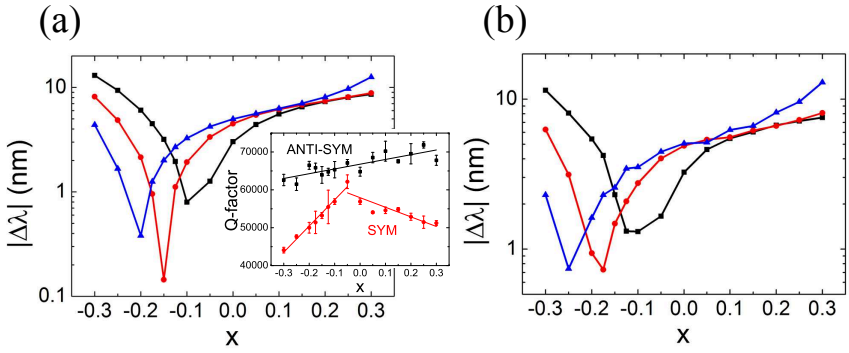


Fig. 5. Dependence of wavelength splitting upon the underlying hole radius r_0. Black: $r_0 = 0.232a$, red: $r_0 = 0.266a$ and blue: $r_0 = 0.3a$. (a) 3D-FDTD simulations and (b) Experimental results. Inset: calculated Q-factors.

#210083 - $15.00 USD Received 14 Apr 2014; accepted 25 Apr 2014; published 13 May 2014
(C) 2014 OSA

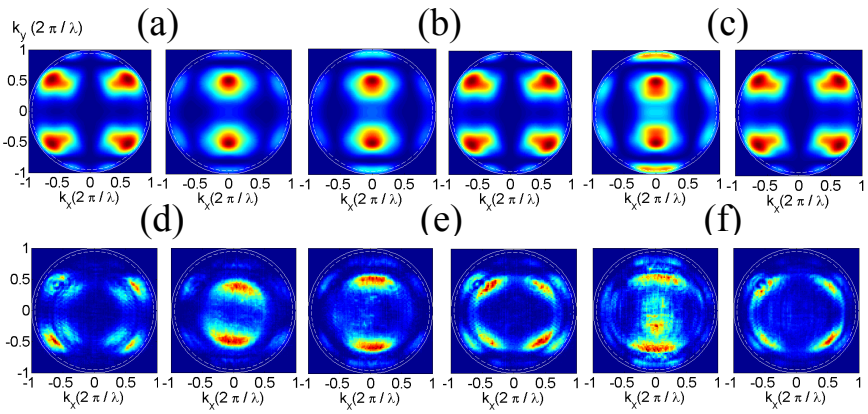


Fig. 6. Far field images from the shortest wavelength mode ($\lambda_<$, left), and the largest wavelength one ($\lambda_>$, right), for different hole sizes in the barrier. (a)-(c) 3D-FDTD simulations, (d)-(f) Experimental results with mean pump power $\sim 35\,\mu W$ on the sample. (a) and (d): $x = -0.15$; (b) and (e): $x = 0$; (c) and (f): $x = 0.15$. Other parameters are the same as in Fig. 4.

4. Experimental results

The fabricated samples are InP-based cavities on a suspended membrane, with resonant modes at around $1.5\,\mu$m. The InP membrane (265 nm-thick), bonded onto a Si substrate, incorporates four central layers of InGaAs/InGaAsP quantum wells (QWs). The QW luminescence at 300 K is centered at $1.52\,\mu$m with a spectral broadening of $\sim$ 80nm. Details on the fabrication can be found in [15].

Scanning Electron Microscopy (SEM) images of cavities with barrier engineering are shown in Fig. 7(a). We have characterized the active cavities via photoluminescence (PL) experiments. Samples are pumped using a Ti:Sa laser emitting 160 fs pulses (80 MHz-repetition rate) at $\lambda =$ 810 nm, through a high numerical aperture microscope objective ($\times$100, N.A.=0.95). PL is collected by the same optics. A spectrometer allows us to spectrally resolve the PL, and an InGaAs camera is used to obtain spatially resolved PL both in the near and far fields, the latter using a lens to image the back-focal plane of the objective. Further details on the experimental setup can be found in [11].

The PL emission shows two resonances as long as the cavities are pumped close to the center (see Fig. 7(b), inset). Laser emission is observed with threshold $\sim 15\,\mu W$. Figure 7(b) shows central wavelengths of splitted modes ($\lambda_<$ and $\lambda_>$) as a function of the middle-row hole size. These measurements allow us to directly obtain the modulus of wavelength splitting [$|\Delta\lambda|$, Fig. 4(d)], showing very good agreement with the numerical simulations [Fig. 4(b)]. In order to define a signed $\Delta\lambda$ in the experiment, we adopt the nomenclature "bonding" and "anti-bonding" used in previous works [11, 15] which, unlike "symmetric" and "anti-symmetric" of Sections 2 and 3, does not suppose any *a priori* rigorous symmetry in the system, it only denotes 0 or π phase difference between cavity fields. The sign of $\Delta\lambda$ is experimentally determined using far-field data. Sharp-edge interference filters ($\sim$ 10 nm-bandpass) are used in order to filter out $\lambda_<$ and $\lambda_>$ modes alternatively. For very small wavelength splitting, $\Delta\lambda < 1$ nm, filters cannot be used. In such cases modes are separated by selective spatial excitation: localizing the excitation spot on one cavity maximizes $\lambda_<$ mode, while $\lambda_>$ is reenforced by exciting the coupled cavity system at the center [11]. Far-field images for $\lambda_<$ and $\lambda_>$ have been measured for all x-parameters of Fig. 4(d) [only $x = \pm 15\%$ and $x = 0$ are shown in Figs. 6(d)–6(f)].

#210083 - $15.00 USD Received 14 Apr 2014; accepted 25 Apr 2014; published 13 May 2014
(C) 2014 OSA

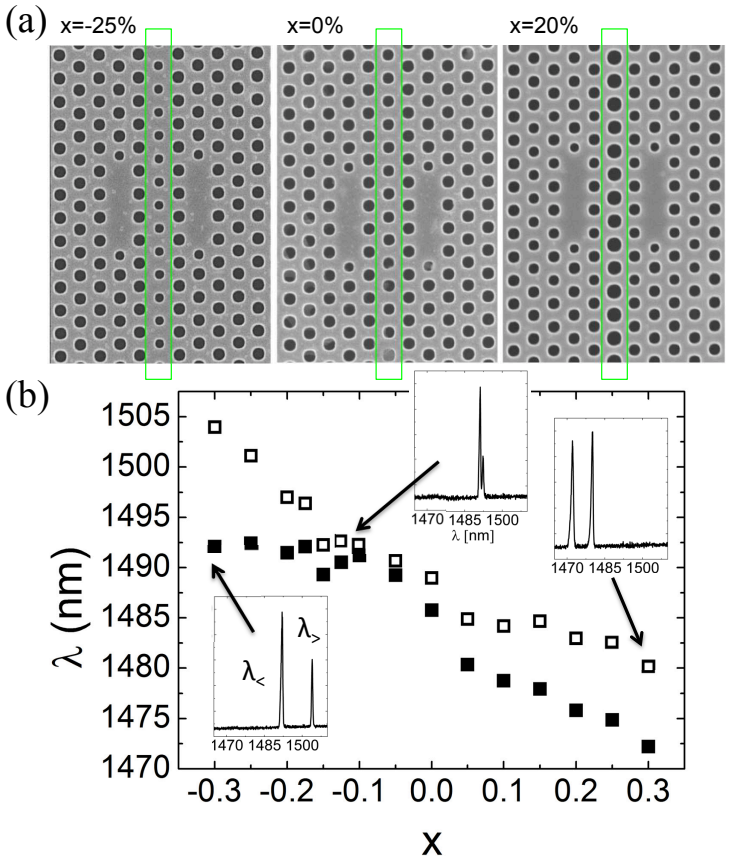


Fig. 7. (a) SEM images of coupled L3 cavities on a suspended membrane with barrier engineering, for three hole sizes in the barrier. (b) Measured resonant wavelengths of splitted modes ($\lambda_<$:filled squares, and $\lambda_>$: empty squares) as a function of the barrier modification. Inset: PL spectra showing mode splitting. Pump power is $\sim 30\mu W$. Target fabrication parameters are those of Fig. 4.

As predicted by the numerical simulations, the order of bonding and anti-bonding modes is reversed close to $x = -10\%$, and can be observed in Fig. 6 when moving from Fig. 6(d) to Fig. 6(e). Such spectral order of modes is used to obtain the sign of $\Delta\lambda$, thus unfolding the raw spectral data. Wavelength splitting is depicted in Fig. 4(c), showing that the minimum of $|\Delta\lambda|$ indeed corresponds to the proximity of a crossing point.

Changing x parameter in Fig. 7(b) is done by moving from one pair of coupled cavities to another one on the buffer, separated by $\sim 40\,\mu m$. Technological imperfections may thus explain the dispersion of $\lambda_{>,<}$ observed in Fig. 7. The impact of fabrication errors on $\Delta\lambda$ [Fig. 4(c)] is, in turn, much weaker. This can be understood from the sensitiveness of optical properties on geometrical parameters such as r_0. Let us assume that r_0 is changing by a small fraction from one pair of coupled cavities to the next one. Then both mode wavelengths $\lambda_{>,<}$ shift by approximately the same amount. Therefore, the splitting $\Delta\lambda$ is not significantly modified.

Finally, let us discuss degeneracy in real coupled cavities. It turns out that mode degeneracy, as reported in Sections 2 and 3 for ideally identical cavities, can hardly be observed in a real system. Strictly speaking, symmetry is always broken due to imperfections, which cause the coupled cavities to be slightly non-identical. Let us call κ coupling rate (which can be pos-

#210083 - $15.00 USD Received 14 Apr 2014; accepted 25 Apr 2014; published 13 May 2014
(C) 2014 OSA

itive or negative by virtue of the barrier engineering technique). We now introduce a small asymmetrical perturbation in the system, such as slightly different surrounding holes for each cavity. For simplicity, we assume that such asymmetry essentially produces a cavity frequency detuning δ, but it does not alter individual cavity Q-factors. Frequency splitting then scales as $\Delta\omega \sim \sqrt{\delta^2 + 4\kappa^2}$. As a result, close enough to the crossing point, $|\kappa| \ll |\delta|$ and the cavities decouple. On the other hand, the condition $|\kappa| > |\delta|$ ensures efficient optical coupling even in a weak coupling regime ($\tau|\kappa| < 1$, where τ is the photon lifetime in the cavity) .

5. Conclusions

We have demonstrated, both numerically and experimentally, barrier engineering in a L3-based photonic crystal molecule. This technique consists in the modification of the radius of the middle row of holes between the cavities. Initial wavelength splitting of about ~ 3nm has been progressively increased up to ~ 9nm, and decreased down to ~ -12nm, i.e. with a maximum five-fold variation upon $\pm$30% of hole size change *x*. In addition, a region of *x*-values close to -10% has been found where the coupling sign is reversed after degeneracy: the symmetric mode is the ground state for smaller radius, while it becomes the excited state for larger radius. The latter is an unusual situation when compared to coupled classical or quantum coupled oscillators. Interesting enough, such fine tuning of the coupling parameter is compatible with high Q-operation, as Q-factors of the order of $Q \sim 5 \times 10^4$ have been numerically found. An extension to ultrahigh-Q-cavities, such as the so-called heterostructure PhC cavities [23], could be carried out.

A simple 2D Fabry-Perot model allowed us to interpret degeneracy (mode crossing) as the matching of the effective refractive index change to the reflectivity phase change of coupled W1 waveguide Bloch modes as they are reflected onto the PhC mirror closing the cavity. This can be achieved with our design thanks to the mode selectivity of the technique. Indeed, barrier engineering mainly affects the refractive index of the symmetric mode, while the one of the antisymmetric one remains essentially unchanged. Our results open the way to the demonstration of rich nonlinear optical phenomena in multiple potential well nano-photonic systems such as Josephson oscillations, spontaneous symmetry breaking and optical self-trapping.

Acknowledgments

This work was supported by the French National Center for Scientific Research (CNRS), the French National Agency for Research (ANR; ANR-12-BS04-0011) and the French RENATECH network.

#210083 - $15.00 USD Received 14 Apr 2014; accepted 25 Apr 2014; published 13 May 2014
(C) 2014 OSA